Inorg. Chem. **2004**, *43*, 1697–1707

Organometallic Complexes as Hole-Transporting Materials in Organic Light-Emitting Diodes

Xiaofan Ren, Bert D. Alleyne, Peter I. Djurovich, Chihaya Adachi,[†] Irina Tsyba, Robert Bau, and Mark E. Thompson*

Department of Chemistry, University of Southern California, Los Angeles, California 90089

Received October 13, 2003

The use of metal complexes *fac*-tris(1-phenylpyrazolato-*N*,$C^{2'}$)cobalt(III) [*fac*-Co(ppz)$_3$], *fac*-tris(*2*-phenylpyridinato-*N*,$C^{2'}$)cobalt(III) [*fac*-Co(ppy)$_3$], and {tris[2-((pyrrole-2-ylmethylidene)amino)ethyl]amine}gallium(III) [Ga(pma)] as materials for hole-transporting layers (HTL) in organic light-emitting diodes (OLEDs) is reported. Co(ppz)$_3$ and Co(ppy)$_3$ were prepared by following literature procedures and isolated as mixtures of facial (*fac*) and meridional (*mer*) isomers. The more stable *fac* isomers were separated from the unstable *mer* forms via column chromatography and thermal gradient sublimation. Crystals of *fac*-Co(ppz)$_3$ are monoclinic, space group $P2_1/c$, with a = 13.6121(12) Å, b = 15.5600(12) Å, c = 22.9603(17) Å, β = 100.5°, V = 4781.3(7) Å^3, and Z = 8. {Tris[2-((pyrrol-2-ylmethylidene)amino)ethyl]amine}gallium [Ga(pma)] was prepared by the reaction of gallium(III) nitrate with the pmaH$_3$ ligand precursor in methanol. Ga(pma) crystallizes in the cubic space group $I\bar{4}3d$ with cell parameters a = 20.2377(4) Å, b = 20.2377(4) Å, c = 20.2377(4) Å, β = 90.0°, V = 8288.6(3) Å^3, and Z = 16. These cobalt and gallium complexes are pale colored to colorless solids, with optical energy gaps ranging 2.6–3.36 eV. A two-layer HTL/ETL (ETL = electron-transporting layer) device structure using *fac*-Co(ppz)$_3$ and *fac*-Co(ppy)$_3$ as the HTL does not give efficient electroluminescence. However, the introduction of a thin layer of a hole-transporting material (*N*,*N*′-bis(1-naphthyl)-*N*,*N*′-diphenylbenzidine, NPD) as an energy "stair-step" and electron/exciton-blocker dramatically improves the device performance. Both *fac*-Co(ppz)$_3$ and *fac*-Co(ppy)$_3$ devices give external quantum efficiencies higher than 1.0%, with brightness 5000 and 7000 Cd/m^2 at 10 V, respectively. Ga(pma) also functions as an efficient interface layer, giving device performances very similar to those of analogous devices using NPD as the interface layer. Stability tests have been carried out for Co(ppz)$_3$/NPD/Alq$_3$ and Co(ppy)$_3$/NPD/Alq$_3$ devices. While *fac*-Co(ppy)$_3$ gave stable OLEDs, the *fac*-Co(ppz)$_3$-based devices had very short lifetimes. On the basis of the experimental results of chemical oxidation of *fac*-Co(ppz)$_3$, the major cause for the fast decay of the *fac*-Co(ppz)$_3$ device is proposed to be the decomposition of *fac*-Co(ppz)$_3^+$ in the HTL layer during the device operation.

Introduction

There has been a growing interest in the use of organic compounds as charge-transporting materials in electronic devices. One type of device that exploits the charge-transporting ability of organic compounds is the organic light-emitting diode (OLED).[1,2] A common OLED structure consists of an ITO (indium tin oxide) anode on glass, a hole-transporting layer (HTL), an electron-transporting layer (ETL) (which often also serves as the emissive layer), and a metal cathode (i.e. glass/ITO anode/HTL/ETL/cathode).[1,2] Holes and electrons are injected into the carrier-transporting materials from the anode and cathode, respectively, and migrate in the presence of the applied electric field to the HTL/ETL interface. The holes and electrons recombine at

* To whom correspondence should be addressed. E-mail: met@usc.edu.
[†] Present address: Department of Photonics Materials Science, Chitose Institute of Science & Technology, 758−65 Bibi, Chitose 066-8655, Japan.

(1) Tang, C. W.; Van Slyke, S. A. *Appl. Phys. Lett.* **1987**, *51*, 913.

(2) (a) Rothberg, L. J.; Lovinger, A. J. *J. Mater. Res.* **1996**, *11*, 3174. (b) Tang, C. W. *Inf. Disp.* **1996**, *10*, 16. (c) Sibley, S.; Thompson, M. E.; Burrows, P. E.; Forrest, S. R. In *Optoelectronic Properties of Inorganic Complexes*"; Roundhill, D. M., Fakler, J., Eds.; Plenum Press: New York. (d) Shoustikov, A.; You, Y.; Thompson, M. E. *IEEE J. Sel. Top. Quantum Electron.* **1998**, *4*, 3. (e) Burrows, P. E.; Gu, G.; Bulovic, V.; Forrest, S. R.; Thompson, M. E. *IEEE Trans. Electron Dev.* **1997**, *44*, 1188. (f) Forrest, S. R.; Burrows, P. E.; Thompson, M. E. In *Organic Electroluminescent Materials and Devices*; Miyata, S., Nalwa, H. S., Eds.; Gordon and Breach: Langhorne, PA, 1996.

10.1021/ic035183f CCC: $27.50
Published on Web 02/07/2004

or near the HTL/ETL interface to give excited molecules, or excitons, which give rise to the electroluminescent (EL) emission. A number of materials, both molecular and polymeric, have been used to prepare OLEDs; however, they all share the same basic mechanism for electroluminescence.

Research efforts have been focused on the design of new molecular materials for use as charge-transporting materials in OLEDs.[3] Although a variety of inorganic complexes have been used in the fabrication of OLEDs, the most extensively studied metal complex has been aluminum tris(8-hydroquinolate) (Alq_3).[4,5] Alq_3 has been used as an electron-transporting, electron-emitting, and host material in doped systems. Homoleptic metal quinolates, with metals such as Zn^{2+}, Be^{2+}, and Ga^{3+}, also exhibit good performance in OLEDs.[6] These metal complexes, however, have been used solely as electron-transporting materials in OLEDs and not as hole transporters. While metal complexes such as metallophthalocyanines and metalloporphyrins have been used as hole-injecting materials,[7] the intrinsically high molar absorptivity ($\epsilon > 10^4$ M^{-1} cm^{-1} throughout the visible spectrum) of these materials leads to excessive absorbance of the OLED emission and, thus, hinders their ability to act as bulk hole transporters. Therefore, the most common hole-transporting materials used for small-molecule-based OLEDs have been organic triarylamine compounds (e.g. *N*,*N*′-bis-(1-naphthyl)-*N*,*N*′-diphenylbenzidine (NPD), *N*,*N*′-bis(*meta*-tolyl)-*N*,*N*′-diphenylbenzidine (TPD), and 4,4′,4″-tris((3-methylphenyl)phenylamino)triphenylamine (*m*-MTDATA)).[8] Triarylamines were originally developed for charge-transporting layers in xerography and have proven to be excellent hole-transporting materials for OLEDs.[9] These compounds have good thermal stabilities and wide optical gaps, making them readily processable and transparent to OLED emission.

Metal complexes are promising candidates to consider for use as hole-transporting materials, since metal ions can both assume multiple oxidation states and have low kinetic barriers for self-exchange reactions.[10] The cationic complex $Ru(bpy)_3^{2+}$ (bpy = 2,2′-bipyridyl) and its derivatives have been used in single-layer device structures.[11] In these devices the Ru(II) complex, in addition to acting as the luminescent material, transports both holes and electrons.[12] Unfortunately, the low optical energy gap for $Ru(bpy)_3^{2+}$ cation makes these complexes practical only for orange to red emitting devices. Also, the ionic nature of the complex makes fabrication of efficient multilayer devices difficult, if not impossible. Our goal is to prepare metal complexes that can function as efficient hole-transporting materials. The complexes should have energy gaps wide enough to be applicable in blue to red OLEDs and physical characteristics (thermal stability, volatility) that are amenable to deposition using standard vacuum deposition techniques. Recently, cyclometalated complexes of Ir(III) have been shown to be effective as both emissive and charge-transporting materials in vapor-deposited OLEDs.[13] However, the high cost associated with iridium makes these complexes more appropriate for use as luminescent dopants and less attractive as bulk charge-transporting materials. Thus, it would be worthwhile to identify similar electroactive complexes that would serve the same purpose as a charge carrier and yet, which would also incorporate less expensive metals into their structures. In this study, we have chosen to investigate tris-cyclometalated Co(III) and Ga(III) complexes tris(1-phenylpyrazolato-*N*,$C^{2'}$)-cobalt(III) [$Co(ppz)_3$], (tris(2-phenylpyridinato-*N*,$C^{2'}$)cobalt-(III) [$Co(ppy)_3$], and {tris[2-((pyrrole-2-yl)methylidene)-amino)ethyl]amine}gallium(III) [Ga(pma)] as HTL materials (Figure 1). We have discovered several characteristics inherent in the cobalt complexes that affect their ability to function as effective charge transport materials and have identified some solutions that allow them to be successfully employed as HTL materials in OLEDs. We have also

(3) (a) Strukelj, M.; Papadimitrakopoulos, F.; Miller, T. M.; Rothberg, L. J. *Science* **1995**, *267*, 1969. (b) Noda, T.; Shirota, Y. *J. Am. Chem. Soc* **1998**, *120*, 9714. (c) Murata, H.; Kafafi, Z. H.; Uchida, M. *Appl. Phys. Lett*. **2002**, *80*, 189. (d) Ma, D.; Wang, G.; Hu, Y.; Zhang, Y.; Wang, L.; Jing, X.; Wang, F.; Lee, C. S.; Lee, S. T. *Appl. Phys. Lett*. **2003**, *82*, 1296.

(4) (a) Tang, C. W.; Van Slyke, S. A.; Chen, C. H. *J. Appl. Phys*. **1998**, *65*, 3610. (b) Shi, J.; Tang, C. W. *Appl. Phys. Lett.* **1997**, *70*, 1665. (c) Tang, C. W.; Van Slyke, S. A.; Chen, C. H. Chen *J. Appl. Phys*. **1989**, *65*, 3610. (d) Van Slyke, S. A.; Chen, C. H.; Tang, C. W. *Appl. Phys. Lett*. **1996**, *69*, 2160. (e) Shoustikov, A.; You, Y.; Burrows, P. E.; Thompson, M. E.; Forrest, S. R. *Synth. Met.* **1997**, *91*, 217.

(5) (a) Anderson, J. D.; McDonald, E. M.; Lee, P. A.; Anderson, M. L.; Ritchie, E. L.; Hall, H. K.; Hopkins, T.; Mash, E. A.; Wang, J.; Thayumanavan, S.; Barlow, S.; Marder, S. R.; Jabbour, G. E.; Shaheen, S.; Kippelen, B.; Peyghambarian, N.; Wightman, R. M.; Armstrong, N. R. *J. Am. Chem. Soc*. **1998**, *120*, 9646. (b) Burrows, P. E.; Shen, Z.; Bulovic, V.; McCarty, D. M.; Forrest, S. R.; Cronin, J. A.; Thompson, M. E. *J. Appl. Phys*. **1996**, *79*, 7991.

(6) (a) Hamada, Y. *IEEE Trans. Electron Dev*. **1997**, *44*, 1208. (b) Hamada, Y.; Kanno, H.; Sano, T.; Fujii, H.; Nishio, Y.; Takahashi, H.; Usuki, T.; Shibata, K. *Appl. Phys. Lett*. **1998**, *72*, 1939. (c) Donze, D.; Pechy, P.; Gratzel, M.; Schaer, M.; Zuppiroli, L. *Chem. Phys. Lett*. **1999**, *315*, 405. (d) Tokito, S.; Noda, K.; Tanaka, H.; Taga, Y.; Tsutsui, T. *Synth. Met.* **2000**, *111*−*112*, 393. (e) Sano, T.; Nishio, Y.; Takahashi, Y.; Usuki, T.; Shibata, K. *J. Mater. Chem*. **2000**, *10*, 157.

(7) Zhu, L.; Tang, H.; Harima, Y.; Yamashita, K.; Ohshita, J.; Kunai, A. *Synth. Met.* **2002**, *126*, 331.

(8) (a) Borsenberger, P. M.; Mey, W.; Chowdry, A. *J. Appl. Phys*. **1978**, *49*, 273. (b) Van Slyke, S. A.; Tang, T. W. U.S. 5,061,569, 1991. (c) Tokito, S.; Tanaka, H.; Okada, A.; Taga, Y. *Appl. Phys. Lett*. **1996**, *69*, 878. (d) Shirota, Y.; Kuwabara, Y.; Inada, H.; Wakimoto, T.; Nakada, H.; Yonemoto, Y.; Kawami, S.; Imai, K. *Appl. Phys. Lett*. **1994**, *65*, 807. (e) O'Brien, D. F.; Burrows, P. E.; Forrest, S. R.; Koene, B. E.; Loy, D. E.; Thompson, M. E. *Adv. Mater*. **1998**, *10*, 1108. (f) Koene, B. E.; Loy, D. E.; Thompson, M. E. *Chem. Mater*. **1998**, *10*, 2235. (g) Hu, N.-X.; Xie, S.; Popovic, Z.; Ong, B.; Hor, A.-M.; Wang, S. *J. Am. Chem. Soc*. **1999**, *121*, 5097.

(9) (a) Klupfel, K.-W.; Sus, O.; Behmenburg, H.; Neugebauer, W. U.S. 3,180,730, 1965. (b) Brantly, T. B.; Contois, I. E.; Fox, C. J. U.S. 3,567,450, 1970. (c) Brantly, T. B.; Contois, I. E.; Fox, C. J. U.S. 3,658,520, 1972.

(10) (a) Marcus, R. A. *J. Chem. Phys*. **1965**, *43*, 679. (b) Newton, M. D.; Sutin, N. *Annu. Rev. Phys. Chem*. **1984**, *35*, 437. (c) Marcus, R. A.; Sutin, N. *Biochim. Biophys. Acta* **1985**, *81*, 265. (d) Sakanoue, K.; Motoda, M.; Sugimoto, M.; Sakaki, S. *J. Phys. Chem. A* **1999**, *103*, 5551.

(11) Rudmann, H.; Rubner, M. F. *J. Appl. Phys.* **2001**, *90*, 4338−4345. Gao, F. G.; Bard, A. J. *J. Am. Chem. Soc*. **2000**, *122*, 7426. Slinker, J.; Bernards, D.; Houston, P. L.; Abruña, H. D.; Bernhard, S.; Malliaras, G. G. *J. Chem. Soc., Chem. Commun.*, in press.

(12) While the $Ru(bpy)_3X_2$-based devices are actually light-emitting electrochemical cells rather than OLEDs, they conduct holes in much the same way that OLED HTLs do.

(13) Adamovich, V. I.; Cordero, S. R.; Djurovich, P. I.; Tamayo, A.; Thompson, M. E.; D'Andrade, B. W.; Forrest, S. R. *Org. Electron.* **2003**, *4*, 77. The devices reported in the following paper utilized single layers of organoiridium complexes; thus, for the OLED to generate light the Ir complex must both conduct charge and emit: Grushin, V. V.; Herron, N.; LeClooux, D. D.; Marshall, W. J.; Petrov, V. A.; Wang, Y. *Chem. Commun.* **2001**, *16*, 1494.

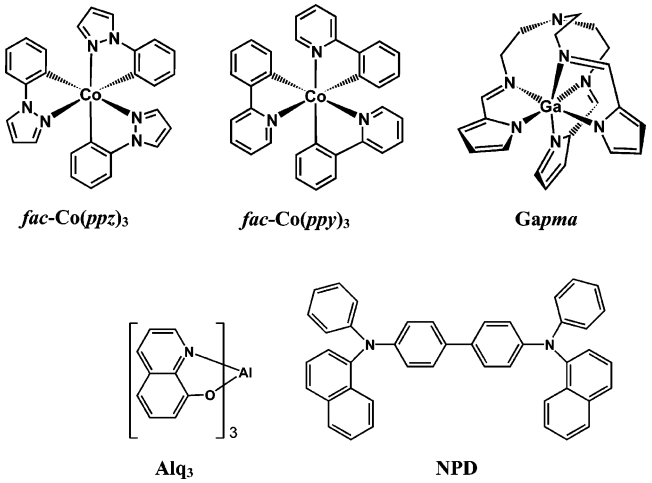

Figure 1. Chemical structures of the compounds used to make OLEDs.

identified a possible chemical origin for the oxidative instability of the *fac*-Co(ppz)$_3$-based HTL films.

Experimental Section

Materials. All starting reagents were purchased from Aldrich Chemical Co., and all syntheses were carried out under an argon or nitrogen atmosphere. Tetrahydrofuran was freshly distilled over sodium/benzophenone prior to use. NPD[14] and aluminum tris(8-hydroquinolate)[15] (Alq_3) were synthesized according to the literature procedures. All materials to be used in device fabrications are further purified by thermal gradient sublimation before being loaded into the chamber, to ensure at least 99% purity.

Equipment. Mass spectra were recorded on an HP 5973 mass spectrometer, using electron ionization at 70 eV. NMR spectra were recorded on Bruker AMX 250, 360, or 500 MHz spectrometers. Absorption spectra were recorded on an Aviv model 14DS UV−vis−IR spectrophotometer and corrected for background solvent absorption. Emission spectra were recorded on a Photon Technology International QuantaMaster model C-60SE spectrofluorometer, equipped with a 928 PMT detector and corrected for detector response. Elemental analyses (C, H, N) were performed at the Microanalysis Lab at the University of Illinois, Urbana-Champaign, IL. The HOMO energies for Co(ppz)$_3$ and Ga(pma) were determined by photoelectron spectroscopy, using an AC-1 (Riken Keiki Co., Japan) UV photoelectron spectrometer.

Electrochemistry. Cyclic voltammetry was carried out in nitrogen-purged anhydrous DMF (Aldrich) at room temperature with an EG&G Princeton potientiostat/galvanostat model 283 interfaced to a PC. The working electrode was a glassy carbon electrode, a Pt wire was used as the counter electrode, and an Ag wire was used as the pseudoreference electrode with ferrocene Fc^+/Fc as the internal standard. Tetrabutylammonium hexafluorophosphate (0.1 M) was used as supporting electrolyte while the concentration of the analyte was 0.1 mM. Cyclic voltammograms were obtained at scan rate of 50 mV. Formal potentials are calculated as the average of cyclic voltammetric anodic and cathodic peaks.

Synthesis of Tris(2-phenylpyrazolato-*N*,*C*$^{2'}$)cobalt(III) [*fac*-Co(ppz)$_3$].[16] Ethylmagnesium bromide (7.6 mL, 7.6 mmol) was added to a solution of 1-phenylpyrazole (1.00 g, 6.93 mmol) in THF (3 mL). The reaction mixture was refluxed for 2 h, under an argon atmosphere, and then cooled in a dry ice/acetone bath. A solution of cobalt(II) bromide (0.76 g, 3.47 mmol) in THF (8 mL) was then added slowly to the Grignard reagent. The bath was removed, and the black mixture was stirred overnight. The reaction mixture was added to aqueous NH_4Cl (10 g/L, 75 mL) and CH_2Cl_2 (75. mL). The resulting thick emulsion was filtered and transferred to a separatory funnel. The organic layer was isolated, and the aqueous layer was extracted twice with CH_2Cl_2. All organic portions were combined, dried over anhydrous $MgSO_4$, filtered, and concentrated under reduced pressure. Addition of hexanes to the yellow/brown concentrate precipitated a dark yellow solid. ^{1}H NMR indicated that the crude product was a mixture of facial and meridional isomers. The two isomers were separated by column chromatography with 1:1 CH_2Cl_2−toluene eluent.[17] Yield: 80.5 mg, 7% (facial isomer). ^{1}H NMR (500 MHz, $CDCl_3$): δ 8.08 (d, 1H, J = 2.6 Hz), 7.15 (dd, 1H, J = 7.7, 1.4 Hz), 6.96 (ddd, 1H, J = 7.5, 7.5, 1.7 Hz), 6.84−6.80 (m, 2H), 6.62 (d, 1H, J = 7.7 Hz), 6.38 (dd, 1H, J = 2.5, 2.5 Hz). MS: *m*/*e* 488 (M^+). Anal. Calcd for $CoC_{27}H_{21}N_6$: C, 66.40; H, 4.30; N, 17.21. Found: C, 66.38; H, 4.26; N, 17.00.

Synthesis of Tris(1-phenylpyridinato-*N*,*C*$^{2'}$)cobalt(III) [*fac*-Co(ppy)$_3$].[18] Magnesium turnings (0.31 g, 12.8 mmol), bromomesitylene (2.50 g, 12.6 mmol), THF (15.0 mL), and a drop of dibromoethane were combined and refluxed gently under argon atmosphere until the magnesium was consumed. The solution was cooled to ca. −30 °C, and a solution of $CoBr_2$ (0.92 g, 4.20 mmol) in THF (7 mL) was then added slowly. Throughout the addition the color of the reaction mixture changed from clear yellow to opaque ochre and finally to yellow/black. The cooling bath was removed, and the mixture was stirred for 1 h. 2-Phenylpyridine (2.18 g, 14.1 mmol) was then added, and the reaction was brought to a gentle reflux for another 1 h. Workup and isolation of the crude product was performed in a manner analogous to that for Co(ppz)$_3$. The crude product was column chromatographed in silica gel using CH_2Cl_2 as eluent. ^{1}H NMR spectroscopy indicated that the sample was a mixture of facial and meridional isomers.[17] Pure facial isomer was obtained by gradient sublimation. ^{1}H NMR (500 MHz, $CDCl_3$): δ 7.86 (d, 1H, J = 7.9 Hz), 7.66−7.61 (m, 2H), 7.28 (d, 1H, J = 7.5 Hz), 6.92 (dd, 1H, J = 7.2, 7.2 Hz), 6.85 (dd, 1H, J = 6.2, 6.2 Hz), 6.81 (dd, 1H, J = 7.2, 7.2 Hz), 6.52 (d, 1H, J = 7.5 Hz). MS: *m*/*e* 521 (M^+). Anal. Calcd for $CoC_{33}H_{24}N_3$: C, 76.00; H, 4.64; N, 806. Found: C, 75.89; H, 4.55; N, 8.09.

Synthesis of {Tris[2-((pyrrol-2-ylmethylidene)amino)ethyl]-amine}gallium(III) [Ga(pma)]. The ligand [((pyrrol-2-ylmethylidene)amino)ethyl]amine was prepared by adding a methanolic solution of pyrrole-2-carboxaldehyde (1.43 g, 15.0 mmol, 100 mL) to a methanolic solution of tris(2-aminoethyl)amine (0.73 g, 5.0 mmol, 10 mL). The resulting yellow solution was stirred at room temperature for 30 min. A methanolic solution of gallium(III) nitrate hydrate (1.28 g, 5.0 mmol, 150 mL) was added to the ligand solution and stirred at room temperature for 30 min. The solution was filtered and left to stand at ambient temperature until crystallization occurred. The crude material was then sublimed at 235 °C. ^{1}H NMR (350 MHz, $CDCl_3$): δ 7.93 (s, 3H), 6.64 (dd, 3H, J = 1.1, 3.3 Hz), 6.19 (dd, 3H, J = 1.7, 3.4 Hz), 6.17 (br s, 3H), 3.45 (ddd, 3H, J = 3.7, 12.7, 12.7), 3.21 (dd, 3H, J = 3.7, 23.93 Hz), 3.17

(14) (a) Drive, M. S.; Hartwig, J. F. *J. Am. Chem. Soc*. **1996**, *118*, 7217. (b) Wolre, J. P.; Wagaw, S.; Buchwald, S. L. *J. Am. Chem. Soc*. **1996**, *118*, 7215.
(15) Schmidbauer, H.; Letterbauer, J.; Kumberger, O.; Lachmann, L.; Muller, G. *Z. Naturforsch*, **1991**, *466*, 1065.
(16) (a) Drevs, H. *Z. Chem*. **1976**, *16*, 493. (b) Marxer, A.; Siegrist, M. *Helv. Chim. Acta* **1974**, *57*, 1988.
(17) Dedeian, K. Ph.D. Dissertation, University of California, Santa Barbara, CA, 1992.
(18) Drevs, H. *Z. Anorg. Allg. Chem*. **1991**, *605*, 145.

Table 1. Crystal Data and Structure Refinement for *fac*-Co(ppz)$_3$·0·5CH$_2$Cl$_2$ ($C_{27}H_{20}N_6Co$·0·5CH_2Cl_2), Ga(pma) ($C_{21}H_{24}N_7Ga$), and Co(ppz$_2$)Cl$_2$ ($C_{18}H_{14}ClN_4Co$)

param	*fac*-Co(ppz)$_3$·0·5CH$_2$Cl$_2$	Ga(pma)	Co(ppz$_2$)Cl$_2$
empirical formula	$C_{27}H_{20}N_6Co$·0·5CH_2Cl_2	$C_{21}H_{24}N_7Ga$	$C_{18}H_{14}ClN_4Co$
fw	530.89	444.1	416.16
temp, K	85(2)	296(2)	273(2)
wavelength (Å)	0.710 73	0.710 73	0.710 73
cryst system	monoclinic	cubic	monoclinic
space group	$P2_1/c$	$I\bar{4}3d$	Pn
unit cell dimens (Å)	a = 13.6121(12)	a = 20.2377(4)	a = 7.866(5)
	b = 15.5600(12)	b = 20.2377(4)	b = 8.854(6)
	c = 22.9603(17)	c = 20.2377(4)	c = 13.619(9)
V (Å^3)	4781.3(7)	8288.6(3)	944.9(11)
Z	8	16	2
density, calcd (Mg/cm^3)	1.475	1.424	1.463
abs coeff (mm^{-1})	0.859	1.350	1.198
F(000)	2184	3680	422
indpndt reflcns	7587 [R(int) = 0.0667]	1586 [R(int) = 0.0392]	3410 [R(int) = 0.0522]
refinement method	full-matrix least squares on F^2	full-matrix least squares on F^2	full-matrix least squares on F^2
data/restraints/params	7587/0/641	1586/0/89	3410/2/226
goodness-of-fit on F^2	1.042	0.964	1.015
final R indices [$I > 2\sigma(I)$]	0.0685	0.0250	0.0298
R indices (all data)	0.1062	0.0288	0.0312

(dd, 3H, J = 3.4, 21.97 Hz), 2.70 (ddd, 3H, J = 3.7, 13.7, 13.7 Hz). MS: *m*/*e* 443 (M^+). Anal. Calcd for $GaC_{21}H_{24}N_7$: C, 56.73; H, 5.40; N, 22.06. Found: C, 56.75; H, 5.50; N, 21.80.

Synthesis of Co[(ppz)$_2$]Cl$_2$. *fac*-Co(ppz)$_3$ (0.2 mmol, 0.098 g) was dissolved in 10 mL of CH_2Cl_2. A 1 equiv amount of (4-BrPh)$_3$N−$SbCl_6$ (0.2 mmol, 0.163 g) was added, and the solution was stirred for 30 min at room temperature under N_2 atmosphere. Concentration of the solution followed by filtration afforded deep blue microcrystals of Co[(ppz)$_2$]Cl$_2$ (yield: ∼50%). Crystals suitable for X-ray crystallography were grown by slow evaporation from a CH_2Cl_2 solution at room temperature.

Density Functional Calculations. DFT calculations were performed using Titan software package (Wavefunction, Inc.) at the B3LYP/LACVP** level. The HOMO and LUMO energies were determined using minimized singlet geometries to approximate the ground state. The minimized singlet geometries were used to calculate the triplet molecular orbitals and approximate the triplet HSOMO (HSOMO = highest singly occupied molecular orbital).

X-ray Crystallography. Diffraction data for the *fac*-Co(ppz)$_3$·0.5CH_2Cl_2, Ga(pma), and Co(ppz$_2$)Cl$_2$ complexes were collected on SMART APEX CCD diffractometer with graphite-monochromated Mo Kα radiation (λ = 0.710 73 Å). The cell parameters for the compounds were obtained from the least-squares refinement of the spots (from 60 collected frames) using SMART program. A hemisphere of the crystal data was collected up to a resolution of 0.75 Å, and the intensity data were processed using the Saint Plus program. All calculations for structure determination were carried out using the SHELXTL package (version 5.1).[19] Initial atomic positions were located by Patterson and direct methods using XS, and the structure was refined by least-squares methods using SHELX. Absorption corrections were applied by using SADABS.[20] Calculated hydrogen positions were input and refined in a riding manner along with the attached carbons. A summary of the refinement details and the resulting factors are given in Table 1.

Device Fabrication and Testing. Prior to device fabrication, ITO with a resistivity of 20 Ω/□ on glass was patterned as 2 mm wide strips. The substrates were cleaned by sonication in soap solution, rinsed with deionized water, boiled in trichloroethylene, acetone, and ethanol for 3−4 min in each solvent, and dried with nitrogen. Finally, the substrates were treated with UV/ozone for 10 min. Organic layers were deposited sequentially by thermal evaporation from resistively heated tantalum boats onto the substrate at a rate of 2.0−3.0 Å/s. The base pressure at room temperature was (3−4) × 10^{-6} Torr. The deposition rate was controlled using a crystal monitor that was located near the substrate. After organic film deposition, the vacuum chamber was vented and a shadow mask with a 2 mm wide stripe was placed onto the substrate and oriented 90° with respect to the ITO stripes. The metal cathode of magnesium silver alloy ($Mg_{0.9}Ag_{0.1}$) was deposited at a rate of 2.2 Å/s capped with a protection Ag layer with the thickness of 400 Å. The devices were tested in air within 2 h of fabrication. Current−voltage measurements were made using a Keithley source meter (model 2400). Light intensity was measured using a Newport model 1835 optical power meter with an 818-UV detector. Only light emitting from the front face of the OLED was collected and used in subsequent efficiency calculations. EL spectra were measured with a Photon Technology International fluorometer.

Device Encapsulation. Devices selected for stability testing were immediately transferred to a N_2-filled glovebox upon fabrication. A thin bead of epoxy adhesive (Epotek, Billerica, MA, No. 730 Epoxy) was applied from a syringe around the edge of the glass substrates, taking care not to make contact between the epoxy and the organic layers. To complete the package, a clean cover glass was placed on top of the device. The epoxy was cured first under intense UV radiation (OAI Collimated UV Lightsources) for 2 min and then was left to fully cure at room temperature for 3 h.

Results and Discussion

Synthesis and Characterization. The cyclometalated cobalt complexes were synthesized using two different routes. The synthesis of *fac*-Co(ppz)$_3$ involved the reaction of anhydrous $CoCl_2$ with (2-pyrazolylphenyl)magnesium bromide, ppzMgBr, which gave *fac*-Co(ppz)$_3$ as well as a number of side products.[16,17] The 1-phenylpyrazolyl Grignard reagent was prepared by orthometalating 1-phenylpyrazole (ppzH) with ethylmagnesium bromide. The *fac*-Co(ppy)$_3$ complex was prepared by a method involving cyclometalation of 2-phenylpyridine (ppyH) with the reactive MgCo(mesitylene)$_3$Br reagent.[18] Here, the three mesitylene anions assist in the cyclometalation reaction of the incoming ligand

(19) Sheldrick, G. M. *SHELXTL*, version5.1; Bruker Analytical X-ray Systems, Inc.: Madison, WI, 1997.
(20) Blessing, R. H. *Acta Crystallogr*. **1995**, *A51*, 33.

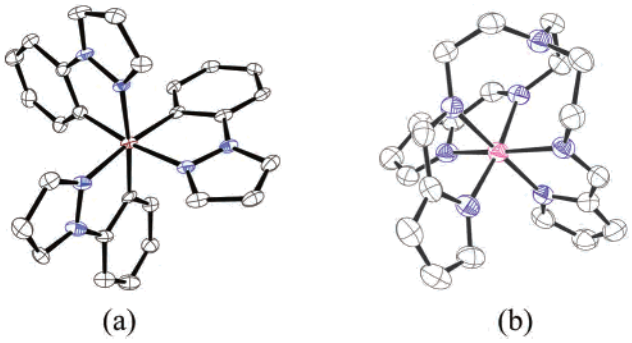

Figure 2. Molecular structures of (a) *fac*-Co(ppz)$_3$ and (b) Ga(pma).

precursors. It has been suggested that both processes involve a disproportion reaction to give the final Co(III) products.[16] Both reactions give low yields (<20%) of the tris-chelated cobalt complexes as a mixture of facial and meridional isomers. Isomer separation was achieved through a combination of column chromatography and vacuum sublimation. For the Co(ppz)$_3$ complex, only the facial isomer elutes from the chromatography column, leaving a purple band at the column head, which is most likely the decomposed meridional isomer. In contrast, the meridional form of Co(ppy)$_3$ is more stable and does not readily decompose during column chromatography. The eluent exiting the column, though richer in the facial isomer of Co(ppy)$_3$, still contained a significant amount of meridional isomer. Therefore, pure samples of *fac*-Co(ppy)$_3$ were obtained by sequential column chromatography and sublimation. The instability of the meridional isomers is most likely due to the strongly trans-directing phenyl groups located opposite each other in the meridional isomer. In the facial isomers of Co(ppz)$_3$ and Co(ppy)$_3$, however, all of the electron-donating phenyl groups are trans to electron accepting pyrazolyl or pyridyl groups. Support for this hypothesis comes from the isoelectronic Ir(ppz)$_3$ and Ir(ppy)$_3$ complexes where both facial and meridional isomers of the complexes can be isolated.[21] The meridional isomer of the Ir tris-cyclometalate is readily converted to the facial isomer either thermally or photochemically, demonstrating that the meridional isomer is the less stable configuration.

The facial isomers of both Co(ppz)$_3$ and Co(ppy)$_3$ are air stable and sublime cleanly. The C_3 symmetry of the complexes is readily apparent from the very simple ^{1}H NMR spectra displayed by both complexes. The ^{1}H NMR spectra of *fac*-Co(ppz)$_3$ and *fac*-Co(ppy)$_3$ display only seven and eight resonances, respectively, consistent with equivalent cyclometalating ligands. The facial configuration of Co(ppz)$_3$ was also confirmed by X-ray crystallographic analysis. The coordination geometry around cobalt is pseudooctahedral, with the three ppz ligands bound in a facial orientation; see Figure 2. There are two unique complexes in the unit cell, making the three phenylpyrazole ligands crystallographically inequivalent. The average Co−C and Co−N bond lengths are 1.921(6) and 1.971(5) Å, respectively, while the average C−Co−N chelate bite angle is ∼83.1(2)°. To our best knowledge, *fac*-Co(ppz)$_3$ is the first crystallographically characterized tris-cyclometalated Co(III) (C^N)$_3$ complex; thus, direct comparison of Co−C and Co−N bond distances with those in other Co(III) (C^N)$_3$ complexes is not possible. Nevertheless, the Co−C bond lengths in *fac*-Co(ppz)$_3$ are close to the average of reported values (1.93 Å) in arylcobalt(III) compounds,[22] whereas the Co−N bond lengths in *fac*-Co(ppz)$_3$ are slightly on the longer side compared to those of reported complexes with the Co(III)−N(pyrazolyl) structure (average = 1.943 Å).[23] The elongation observed here is most likely due to the trans effect imposed by the electron-donating phenyl groups located in the opposite position. In addition, the bond lengths are smaller than the average Ir−C (2.021(6) Å) and Ir−N (2.124(5) Å) bond lengths found in *fac*-Ir(ppz)$_3$,[21] reflecting the smaller size of the Co atom. Attempts to grow single crystals of *fac*-Co(ppy)$_3$ suitable for X-ray crystallographic analysis have not been successful.

The Ga(III) complex, Ga(pma) (Figure 1), was prepared using a procedure similar to that described by Katsuki et al. in the synthesis of first-row transition metal complexes with imidazole analogues.[24] The pmaH$_3$ ligand precursor was prepared by a reaction of a methanolic solution of pyrrole-2-carboxaldehyde with tris(2-aminoethyl)amine.[25] Stirring pmaH$_3$ with gallium(III) nitrate hydrate in methanol at room temperature forms Ga(pma), which upon standing precipitates out of solution as colorless crystals. The crystal structure for Ga(pma) shows the gallium in a pseudooctahedral geometry coordinated by imine and pyrrole nitrogens (Figure 2); i.e., cis angles are in the range of 79.0−96.5° and trans angles are on average 172°. The Ga−N bond lengths range from 2.014(1) to 2.115(1) Å, with the short distances being those to the anionic pyrrole nitrogens.

Electronic Spectroscopy. The UV/vis spectra of *fac*-Co(ppz)$_3$ and *fac*-Co(ppy)$_3$ are shown in Figure 3. High-energy, intense UV absorption bands (λ_{max} = 270−310 nm, $\epsilon = 3.0 \times 10^4$ M^{-1} cm^{-1}) are assigned to a metal-perturbed $\pi \rightarrow \pi^*$, ligand-centered (LC) transition by comparison with the absorption spectra of the free ligands ppzH and ppyH. Lower energy absorption bands are observed for both *fac*-Co(ppz)$_3$ (λ_{max} = 345 nm, ϵ = 7500 M^{-1} cm^{-1}) and *fac*-Co(ppy)$_3$ (λ_{max} = 440 nm, ϵ = 8000 M^{-1} cm^{-1}). Each of these bands displays solvatochromic behavior, shifting to higher energies in more polar solvents. The absence of absorption in the same spectral region for the protonated ligand precursors, the

(21) Tamayo, A.; Alleyne, B. D.; Djurovich, P. I.; Lamansky, S.; Tsyba, I.; Bau, R.; Thompson, M. E. *J. Am. Chem. Soc.* **2003**, *125*, 7377.

(22) (a) Robitzer, M.; Sirlin, C.; Kyritsakas, N.; Pfeffer, M. *Eur. J. Inorg. Chem.* **2002**, *9*, 2312. (b) Meneghetti, M. R.; Grellier, M.; Pfeffer, M.; De Cian, A.; Fischer, J. *Eur. J. Inorg. Chem.* **2000**, *7*, 1539. (c) Meneghetti, M. R.; Grellier, M.; Pfeffer, M.; Dupont, J.; Fischer, J. *Organometallics* **1999**, *18*, 5560.

(23) (a) Saha, N. C.; Butcher, R. J.; Chaudhuri, S.; Saha, N. *Polyhedron* **2003**, *22*, 383. (b) Barik, A. K.; Paul, S.; Butcher, R. J.; Kar, S. K. *Polyhedron* **2000**, *19*, 2651. (c) Higgs, T. C.; Ji, D.; Czemuscewicz, R. S.; Carrano, C. J. *Inorg. Chim. Acta* **1999**, *286*, 80. (d) Matthews, H. R.; Bucke, L. C.; Blackman, A. G. *Inorg. Chim. Acta*, **1998**, *277*, 89. (e) Higgs, T. C.; Ji. D.; Czemuszewicz, R. S.; Matzanke, B. F.; Schunemann, V.; Trautwein, A. X.; Helliwell, M.; Ramirez, W.; Carrano, C. J. *Inorg. Chem.* **1998**, *37*, 2383. (f) Chavez, F.; Olmstead, M. M.; Mascharak, P. K. *Inorg. Chem.* **1997**, *36*, 6323.

(24) (a) Katusuki, I.; Matsumoto, N.; Kojila, M. *Inorg. Chem.* **2000**, *39*, 3350. (b) Katsuki, I.; Motoda, Y.; Sunatsuki, Y.; Matsumoto, N.; Nakashima, T.; Kojima, M. *J. Am. Chem. Soc.* **2002**, *124*, 629.

(25) Sim, P. G.; Sinn, E. *Inorg. Chem.*, **1978**, *17*, 1288.

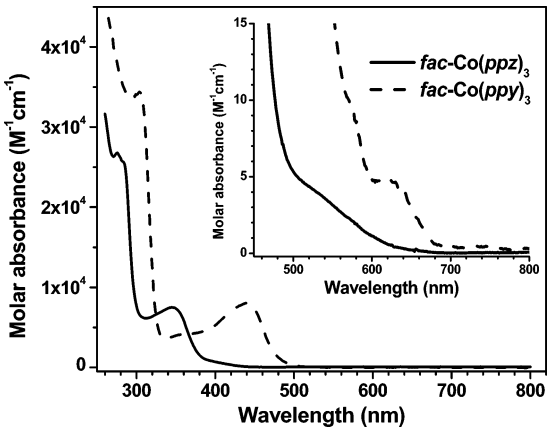

Figure 3. Absorption spectra of *fac*-Co(ppz)$_3$ and *fac*-Co(ppy)$_3$ in dichloromethane.

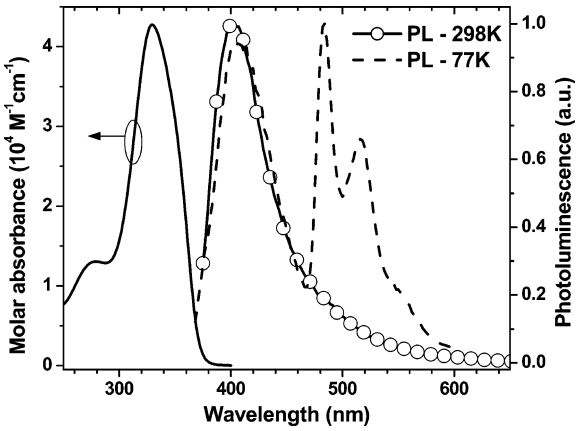

Figure 4. Absorption and emission spectra of Ga(pma) at room temperature and 77 K.

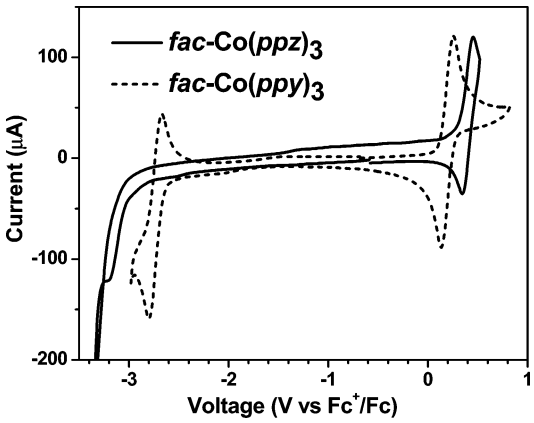

Figure 5. Cyclic voltammograms of *fac*-Co(ppz)$_3$ and *fac*-Co(ppy)$_3$ in DMF. Scan rate: 50 mV/s. Electrolyte: 0.1 M tetrabutylammonium hexafluorophosphate.

strong molar absorptivity of the bands, and the fact that they are solvatochromic suggest a metal-to-ligand charge-transfer (MLCT) assignment for these transitions. The absorption spectra of *fac*-Co(ppz)$_3$ and *fac*-Co(ppy)$_3$ also display very weak ($\epsilon = 1-50$ M^{-1} cm^{-1}), low-energy bands that extend throughout the visible region (Figure 3, inset). These absorption features give rise to the yellowish color of the *fac*-Co(ppz)$_3$ compound and are most likely due to d−d transitions that are characteristic of octahedral Co(III) complexes. The cyclometalated cogeners made with the heavier elements, *fac*-Ir(ppz)$_3$, *fac*-Ir(ppy)$_3$, or *fac*-Rh(ppy)$_3$, display no such absorption features at wavelengths longer than the MLCT transition.[21,26] The d−d transition bands in the Ir and Rh analogues are most likely at higher energy under the more intense MLCT transitions. It is noteworthy that the d−d transitions of *fac*-Co(ppz)$_3$ and *fac*-Co(ppy)$_3$ occur at much higher energy than values found in other Co(III) N^N chelate complexes (<690 nm),[27] which indicates that the anionic cyclometalating ligands have a large ligand field strength. However, the ligand field splitting is not sufficiently large to prevent excited-state deactivation since, unlike the behavior of cyclometalated Ir(III) and Rh(III) complexes, no detectable emission was observed for *fac*-Co(ppz)$_3$ and *fac*-Co(ppy)$_3$ at either room temperature or 77 K. Luminescence quenching by similar low energy d−d states is also responsible for the absence of MLCT emission in Fe(bpy)$_3^{2+}$ complexes.[28]

The absorption and emission spectra of Ga(pma) are shown in Figure 4. A broad absorption band ($\lambda_{max} = 330$ nm, $\epsilon = 4 \times 10^4$ M^{-1} cm^{-1}) closely matches the absorption spectrum of the protonated ligand precursor and thus is assigned as a ligand-based $\pi \rightarrow \pi^*$ transition. At ambient temperature, Ga(pma) fluoresces weakly in THF solution. The broad emission band has a maximum at 423 nm with a long tail extending beyond 500 nm. Upon cooling of the sample to 77 K, a new emission band is seen in addition to the fluorescence band. This band, which displays a vibronic progression of 1280 cm^{-1}, has a maximum at 480 nm and is assigned to a metal-perturbed, $\pi^* \rightarrow \pi$ phosphorescent transition of the pma ligand.

Electrochemistry and Ultraviolet Photoelectron Spectroscopy (UPS). Electrochemical analysis by cyclic voltammetry shows that *fac*-Co(ppz)$_3$ exhibits a reversible oxidation at 0.40 V, while a reversible oxidation of *fac*-Co(ppy)$_3$ occurs at 0.19 V (in DMF vs Fc$^+$/Fc; see Figure 5). These oxidation waves can be assigned to formal Co(IV)/Co(III) couples, given the high donor capacity and insensitivity of both the ligands toward oxidation. Reversible oxidative behavior in what are formally Co(III) complexes is extremely rare. Chemical and electrochemical oxidations of organocobalt complexes have been reported, and stable Co(IV) species have been isolated.[29] However, nearly all prior organocobalt complexes with reversible Co(IV)/Co(III) couples contain polydentate ligands which have extensive π-electron systems, such as the tetradentate dianions derived from Schiff bases or α-dioximes.[30] The existence of such

(26) Columbo, M. G.; Brunold, T. C.; Riedener, T.; Güdel, H. U.; Förtsch, M.; Bürgi, H.-B. *Inorg. Chem.* **1994**, *33*, 545.
(27) Hancock, R. D.; McDougall, G. J. *J. Chem Soc., Chem. Commun.* **1977**, 67.
(28) (a) Fink, D. W.; Ohnesorge, W. E. *J. Am. Chem. Soc.* **1969**, *91*, 4995. (b) Creutz, C.; Chou, M.; Netzel, T. L.; Okumura, M.; Sutin, N. *J. Am. Chem. Soc.* **1980**, *102*, 1309.
(29) (a) Anson, F. C.; Collins, T. J.; Coots, R. J.; Gipson, S. L.; Richmoond, T. G. *J. Am. Chem. Soc.* **1984**, *106*, 5037. (b) Byrne, E. K.; Theopold, K. H. *J. Am. Chem. Soc.* **1987**, *109*, 1282. (c) Collins, T. J.; Powell, R. D.; Slebodnick, C.; Uffelman, E. S. *J. Am. Chem. Soc.* **1991**, *113*, 8419. (d) Chopra, M.; Hum, T. S. M.; Leung, W.-H.; Yu, N.-T. *Inorg. Chem.* **1995**, *34*, 5973.

formal Co(IV) states is rather unusual in organocobalt complexes with only bidentate ligands.[17] In the present case, DFT calculations show a HOMO that consists of a mix of metal and phenyl orbital character that is similar to the picture determined for the analogous Ir cyclometalates.[31] The potentials are similar to values that are found for reversible oxidation couples in *fac*-Ir(ppz)$_3$ (0.40 V) and *fac*-Ir(ppy)$_3$ (0.30 V). Therefore, the oxidative electrochemistry of the cyclometalated Co complexes is most likely a consequence of the Co−phenyl linkage. A reversible reduction wave is observed at −2.66 V for *fac*-Co(ppy)$_3$, whereas the *fac*-Co(ppz)$_3$ complex undergoes irreversible reduction at −3.1 V. These reductions occur at significantly more negative potentials than are found for typical Co(III/II) couples[32] and thus, do not represent direct reduction of the Co center. The reduction of cyclometalated Co complexes can instead be assigned to reduction of the ppy and ppz ligands in analogy to a similar process observed in *fac*-Ir(ppy)$_3$ and *fac*-Ir(ppz)$_3$ at −2.7 and −3.1 V, respectively.[21]

While electrochemical studies establish relative potentials and stabilities of oxidized or reduced materials, it is not the preferred method for determining the HOMO or LUMO energies relative to vacuum needed for OLED design.[33] The best method to evaluate the HOMO energy of a given material in the solid state is ultraviolet photoelectron spectroscopy (UPS). This technique gives a direct measure of the HOMO energy. UPS measurements of *fac*-Co(ppz)$_3$ indicate the HOMO level lies at 5.3 eV. Using this UPS data and the difference in oxidation potentials between the two Co(C^N)$_3$ complexes, the HOMO level for *fac*-Co(ppy)$_3$ is estimated to be at 5.1 eV. By subtraction of the electrochemical redox energy gap (2.85 eV) from the HOMO energy, the LUMO energy for *fac*-Co(ppy)$_3$ is estimated at 2.25 eV. Likewise, for *fac*-Co(ppz)$_3$, if the value of the cathodic half-wave of the irreversible reduction is used for the estimation, the LUMO value is 1.8 eV. To define the energy of the LUMO accurately, one needs an unambiguous value for the optical gap that correlates with well-defined redox potentials. Generally, the optical gap of a given compound is taken as the intersection point of its absorption and emission spectra. However, for *fac*-Co(ppz)$_3$ and *fac*-Co(ppy)$_3$, the optical gap is not easily quantified since only the absorption spectrum is available in both cases. If the low-energy edges at the absorption bands for *fac*-Co(ppz)$_3$ (425 nm) and *fac*-Co(ppy)$_3$ (480 nm) are used for the optical gap calculation, the HOMO−LUMO optical gaps can be estimated as 3.0 and 2.6 eV, respectively. Accordingly, the LUMO energies can be given the values 2.3 and 2.5 eV for *fac*-Co(ppz)$_3$ and *fac*-Co(ppy)$_3$, respectively (on the basis of the HOMO energies of 5.3 and 5.1 eV). The true values for their LUMO energies most likely lie between these limits (i.e., 1.8−2.3 eV for Co(ppz)$_3$ and 2.25−2.5 eV for Co(ppy)$_3$). The relative energies as well as those for NPD and Alq$_3$ are shown schematically in Figure 6.

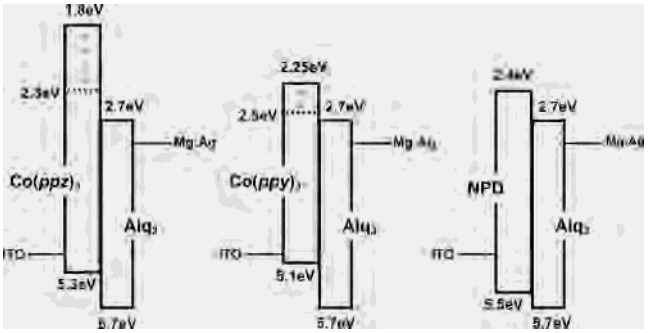

Figure 6. Energy diagrams for *fac*-Co(ppz)$_3$, *fac*-Co(ppy)$_3$ and NPD OLEDs. The dotted lines indicate the LUMO energies based on the optical absorption spectra, while the solid lines (1.8 and 2.25 eV for Co(ppz)$_3$ and Co(ppy)$_3$, respectively) are based on electrochemical measurements.

The Ga(pma) complex undergoes irreversible oxidation and reduction at 0.51 V and −2.84 V (in DMF, vs Fc^+/Fc), respectively. A DFT calculation of Ga(pma) shows the HOMO to be localized primarily on the pyrrolyl rings and not the tertiary ammine. The electrochemical gap based on these irreversible couples (3.35 eV) corresponds well with the optical gap, defined here as the intersection of the absorption and emission spectra (370 nm, 3.36 eV). The value of the HOMO energy measured by UPS is 5.7 eV, and thus, the LUMO energy of Ga(pma) is estimated to be 2.35 eV.

OLED Studies. The first OLEDs prepared with *fac*-Co(ppz)$_3$ and *fac*-Co(ppy)$_3$ were simple two-layer, single heterostructure devices. The triarylamine used for comparative purposes was NPD, a standard HTL material for small-molecule-based OLEDs, while the electron-transporting and emissive layer was composed of Alq$_3$. The device structure was ITO/HTL (500 Å)/Alq$_3$ (500 Å)/Mg:Ag, where the HTL was either NPD or one of the two cobalt complexes. Figure 7 displays the current−voltage characteristics for the various devices. At a given bias, a similar amount of current was passed through the *fac*-Co(ppy)$_3$ device compared to the standard NPD device, whereas much less current passed through the *fac*-Co(ppz)$_3$ device. The external quantum efficiency (EQE) for the *fac*-Co(ppz)$_3$ device reached only 0.3%, compared to 0.8% for the standard NPD-based device (Figure 7, inset), while the quantum efficiency of the *fac*-Co(ppy)$_3$ device was extremely poor (∼0.02%), with the light intensity never rising above 35 Cd/m^2.[34]

(30) (a) Costa, G.; Puxeddu, A.; Reisenhofer, E. *J. Chem. Soc., Dalton Trans.* **1972**, 1519. (b) Levitin, I. Y.; Sigan, A. L.; Vol'pin, M. E. *J. Organomet. Chem.* **1976**, *114*, C53. (c) Muller, E.-Ch.; Kraft, R.; Etzold, G.; Drevs, H.; Taube, R. *J. Prakt. Chem.* **1978**, *320*, 49. (d) Chum, H. L.; Rabockai, T.; Dockal, E. R.; Benedetti, A. V. *J. Electroanal. Chem.* **1979**, *98*, 283. (e) Vol'pin, M. E.; Levitin, I. Y.; Sigan, A. L.; Halpern, J.; Tom, G. M. *Inorg. Chim. Acta* **1980**, *41*, 271. (f) Benedetti, A. V.; Dockal, E. R.; Chum, H. L.; Rabockai, T. *J. Electroanal. Chem.* **1982**, *133*, 45. (g) Benedetti, A. V.; Dockal, E. R.; Chum, H. L.; Rabockai, T. *J. Electroanal. Chem.* **1982**, *142*, 191. (h) Datta, D.; Sharma, T. G. *J. Chem. Soc., Dalton Trans.* **1989**, *1*, 115. (i) Fukuzumi, S.; Miyamoto, K.; Suenobu, T.; Caemelbecke, E. V.; Kadish, K. M. *J. Am. Chem. Soc.* **1998**, *120*, 2880.

(31) Hay, P. J. *J. Phys. Chem. A* **2002**, *106*, 1634.

(32) (a) Böttcher, A.; Takeuchi, T.; Hardcastle, K. I.; Meade, T. J.; Gray, H. B. *Inorg. Chem.* **1997**, *36*, 2498. (b) Richert, S. A.; Tsang, P. K. S.; Sawyer, D. T. *Inorg. Chem.* **1989**, *28*, 2471.

(33) Richardson, D. E. *Inorg. Chem.* **1990**, *29*, 3213.

(34) The candela (Cd) is the luminous intensity, in a given direction, of a source that emits monochromatic radiation of frequency 540×10^{12} Hz and that has a radiant intensity in that direction of 1/683 W/steradian. The luminous intensity of a light source is defined by multiplying the watts emitted at each wavelength by the efficiency of that wavelength in exciting the eye, relative to the efficiency at 555 nm. This efficiency factor is referred to as the V-lambda curve. For Alq$_3$ emission, 1 Cd/m^2 = 10000 × 683 × 0.18 W/cm^2.

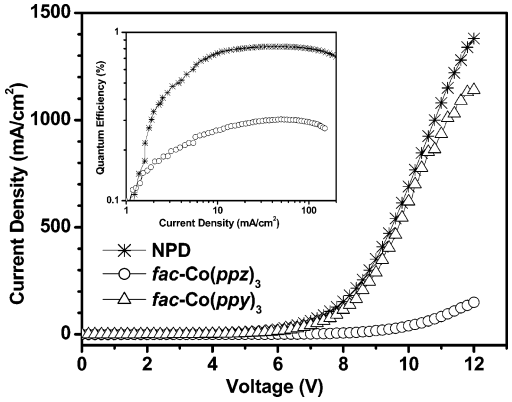

Figure 7. Current−voltage curves for *fac*-Co(ppz)$_3$, *fac*-Co(ppy)$_3$, and NPD OLEDs. Inset: External quantum efficiency−voltage curves for *fac*-Co(ppz)$_3$ and NPD OLEDs. The device structure was ITO/HTL (500 Å)/Alq$_3$ (500 Å)/Mg:Ag.

The difference in performance between the two Co(C^N)$_3$ complexes can be rationalized by comparing the relative HOMO and LUMO energies of the OLED materials (Figure 6). While there is a 0.4 eV energy offset between the HOMOs of *fac*-Co(ppz)$_3$ and Alq$_3$, there exists a 0.6 eV energy offset between the HOMOs of *fac*-Co(ppy)$_3$ and Alq$_3$. Both of these offsets are larger than the 0.2 eV offset expected between NPD and Alq$_3$. Such a large energy offset is expected to lead to an increased barrier for migration of holes from the HTL to Alq$_3$. Moreover, the smaller energy offset between the LUMO levels of *fac*-Co(ppy)$_3$ and Alq$_3$ (0.45−0.20 eV), relative to that of HOMOs, may lead to excessive electron leakage into the Co(ppy)$_3$ layer and thereby shift recombination zone into the nonemissive *fac*-Co(ppy)$_3$ layer. A similar electron leakage in the *fac*-Co(ppz)$_3$ device is presumably blocked by a higher LUMO energy of *fac*-Co(ppz)$_3$. While we were unable to define the LUMO position for *fac*-Co(ppz)$_3$ definitively (vide supra), a value close to the upper limit of 1.8 eV would certainly lead to an effective barrier to electron leakage into the *fac*-Co(ppz)$_3$ layer. While electrons may be blocked from diffusing into the *fac*-Co(ppz)$_3$ layer, energy transfer caused by exciton diffusion into the HTL and subsequent quenching by the nonemissive *fac*-Co(ppz)$_3$ molecules is another likely loss mechanism leading to lower efficiency than that of the NPD-based device. Therefore, the energetics of the Co(C^N)$_3$/Alq$_3$ interface prevent efficient performance of the Co(C^N)$_3$-based OLEDs.

To eliminate electron and/or exciton leakage and improve carrier recombination in the Co(C^N)$_3$ complex based devices, OLEDs were prepared with a trilayer structure in which a thin NPD layer was inserted between *fac*-Co(ppz)$_3$ or *fac*-Co(ppy)$_3$ HTL and Alq$_3$ layer. A previous study demonstrated the utility of such an interlayer when *N*,*N*′-iminostilbenyl-4,4′-fluorene (ISF) was used as the hole-transporting material. The NPD interfacial layer was found to both increase the device efficiency and reduce the operating voltage.[35] The HOMO level of NPD is intermediate between those of ISF and Alq$_3$, forming an energetic "stair-step", which facilitates hole migration from the HTL to Alq$_3$. Since the HOMO energy of ISF is similar to the value determined for *fac*-Co(ppy)$_3$, an interlayer should then also improve the device performance of *fac*-Co(ppy)$_3$. In addition, the wide energy gap of NPD acts to effectively block the diffusion of both electrons and exctions from Alq$_3$ into the Co(III) HTL layer. Indeed, both *fac*-Co(ppz)$_3$ and *fac*-Co(ppy)$_3$ devices with an NPD interfacial layer, (ITO/HTL (400 Å)/NPD (100 Å)/Alq$_3$ (500 Å)/Mg:Ag), yielded maximum EQEs above 1.0% (Figure 8) and had turn-on voltages of 3.7 V (voltage at 1 Cd/m^2). The brightness for the Co(ppz)$_3$/NPD and Co(ppy)$_3$/NPD devices reached 5000 and 7000 Cd/m^2 at 10 V, respectively. Moreover, the introduction of NPD layer did not appreciably change the current−voltage characteristics of the *fac*-Co(ppz)$_3$ device but did significantly decrease the current injected into the *fac*-Co(ppy)$_3$ device (Figure 8). The three layer device performance for the *fac*-Co(ppy)$_3$-based device suggests that both electron and exciton leakage into the Co complex layer is responsible for the low EQE in the two-layer *fac*-Co(ppy)$_3$ devices. The NPD layer in these devices most likely acts as not only an efficient electron/exciton-blocking layer between the HTL and Alq$_3$, but also a good energy "stair-step", facilitating hole injection from *fac*-Co(ppy)$_3$ into the Alq$_3$ layer. The poor performance for the two-layer *fac*-Co(ppz)$_3$-based device is thought to be due to exciton leakage only, since the current is low with and without an NPD interface layer.

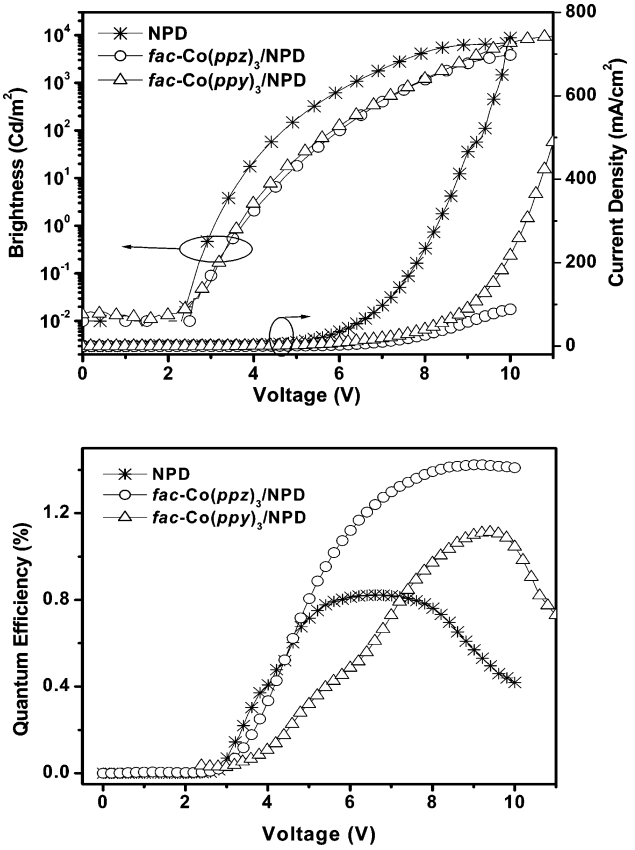

Figure 8. Current−voltage and brightness−voltage curves (top) and external quantum efficiency−voltage curves (bottom) for *fac*-Co(ppz)$_3$, *fac*-Co(ppy)$_3$, and NPD OLEDs. The device structure was ITO/HTL (400 Å)/NPD (100 Å)/Alq$_3$ (500 Å)/Mg:Ag.

(35) Loy, D. E.; Koene, B. E.; Thompson, M. E. *Adv. Funct. Mater.* **2002**, *12*, 245.

The current levels observed for both the *fac*-Co(ppy)$_3$ and *fac*-Co(ppz)$_3$ devices with an NPD interface layer are markedly lower than the reference device (i.e. ITO/NPD/Alq$_3$/cathode), at the same bias. The lower current levels for the two devices with Co-based HTLs suggests that the Co complexes have lower hole mobilities than that of NPD. Alternatively, less efficient hole injection from ITO into the Co complex layers may also contribute to the low current levels observed for the devices with Co complex based HTLs. The best resolution of this issue will involve hole mobility measurements, which are currently underway.

Once the NPD layer was shown to improve the Co(C^N)$_3$/Alq$_3$ device performance, a metal-based alternative to NPD, Ga(pma), was used as an HTL interlayer material. Both the HOMO (5.7 eV) and LUMO (2.35 eV) energies of Ga(pma) are similar to those of NPD, and therefore, Ga(pma) can be expected to function as an efficient interface layer and replace NPD in the device. Note however, that unlike the Co(C^N)$_3$ complexes, the hole-transporting properties of Ga(pma) principally involve the pyrrolyl ligands and not the Ga(III) center. Devices with structure ITO/HTL (400 Å)/Ga(pma) (100 Å)/Alq$_3$ (500 Å)/Mg:Ag were prepared and tested (see Supporting Information). The device properties for these OLEDs were very similar to those described above for NPD interlayer devices (i.e. ITO/HTL/NPD/Alq$_3$/MgAg). The electroluminescence spectra of both devices matched the Alq$_3$ emission spectrum. The turn-on voltages for both *fac*-Co(ppz)$_3$ and *fac*-Co(ppy)$_3$ devices were 3.8 V. Maximum external quantum efficiencies of 1.2% and 1.0% were realized in the *fac*-Co(ppz)$_3$ and *fac*-Co(ppy)$_3$ devices, respectively. At 10 V, the Co(ppz)$_3$ device had a brightness of 3700 Cd/m^2, and the Co(ppy)$_3$ device had a brightness of 5130 Cd/m^2. Therefore, Ga(pma) is an effective electron/exciton-blocking, hole-transporting material for the devices studied here. The high LUMO energy (2.3 eV) of the complex effectively blocks the leakage of electrons to the anode, while the HOMO energy has the appropriate value to promote efficient hole injection.

Device Stability. Stability tests were carried out encapsulated for *fac*-Co(ppz)$_3$/NPD/Alq$_3$ and *fac*-Co(ppy)$_3$/ NPD/Alq$_3$ devices. Both devices were tested at room temperature under nitrogen. During the tests, each device was driven at constant current density of 10 mA/cm^2. Figure 9 shows the luminescence and voltage changes with time for the devices during the first 10 h of device operation. Despite the similarity of their performances as HTLs in this trilayer architecture, the device stabilities based on the two Co(C^N)$_3$ materials are quite different. For the *fac*-Co(ppy)$_3$ device, the light output decreased to 88% of its initial value after 10 h, accompanied by a voltage increase to 1.2 times of its initial value. This behavior is comparable to that of an NPD/Alq device reported in the literature when operated under the same conditions.[36] In the case of *fac*-Co(ppz)$_3$-based device, however, the luminescence dropped to half of its initial value in just 1.5 min and after 12 min, no luminescence was detected. Concomitant with the luminescence decay, a steep voltage rise was also observed, increasing from 8 to 17.5 V in 12 min. Such a rapid voltage increase could be due to a number of factors, including charge trapping and subsequent polarization of the organic layers. Alternatively, an unstable interface between *fac*-Co(ppz)$_3$ and either the anode or Alq$_3$ could cause rapid degradation that consequently impedes carrier injection. To test the latter hypothesis, another device was fabricated and tested with the *fac*-Co(ppz)$_3$ layer imbedded in the NPD film, away from either the ITO or Alq$_3$ interfaces. This device, having the structure ITO/NPD (100 Å)/Co(ppz)$_3$ (400 Å)/NPD (100 Å)/Alq (500 Å)/Mg:Ag, gave a similar degradation response during operation to that of the *fac*-Co(ppz)$_3$-based device described above. Therefore, it is possible to rule out instability of the ITO/Co(ppz)$_3$ interface as the cause of the rapid degradation of *fac*-Co(ppz)$_3$-based devices.

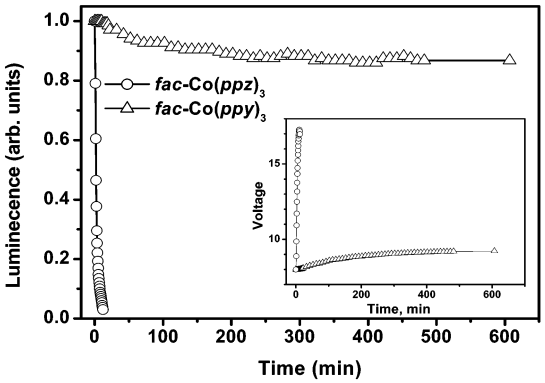

Figure 9. Stability study of *fac*-Co(ppz)$_3$- and *fac*-Co(ppy)$_3$-based devices, operating at constant current of 10 mA/cm^2. The device structure used here was ITO/CoX$_3$ (400 Å)/NPD (100 Å)/Alq$_3$ (500 Å)/Mg:Ag.

Charge trapping is a common phenomenon during OLED operation and leads to low polaron mobility.[37] If the "detrapping" energy required is not available to promote the hole to an adjacent molecule, decomposition of the trapped polaron may occur. Furthermore, dipole rearrangement induced by electric field may also promote the decomposition of the polaronic species. Thus, although *fac*-Co(ppz)$_3^+$ is stable on the time scale of a cyclic voltammetric experiment, molecular structural rearrangement and decomposition might still occur in an operating EL device.

To investigate the stability of *fac*-Co(ppz)$_3^+$, we attempted to prepare and isolate the cation. *fac*-Co(ppz)$_3$ with 1 equiv of (4-BrPh)$_3$N−SbCl$_6$ ($E_{1/2}$ = + 0.7 V vs Fc$^+$/Fc) in CH_2Cl_2 was stirred under an inert atmosphere for 30 min at room temperature. Concentration of the solution followed by filtration afforded deep blue microcrystals (yield: ∼50%). Crystals suitable for X-ray crystallography were grown by slow evaporation from a CH_2Cl_2 solution at room temperature. The structure analysis reveals that the product is not the expected *fac*-Co(ppz)$_3^+$ but a four coordinate Co(II) complex, Co(ppz$_2$)Cl$_2$ (Figure 10, inset). The structure consists of a slightly distorted tetrahedral geometry around the metal center. Two pyrazolyl nitrogens and two chlorine

(36) dos Anjos, P. N. M.; Aziz, H.; Hu, N.-X.; Popovic, Z. D. *Org. Electron.* **2002**, *3*, 9.
(37) Kondakov, D. Y.; Sandifer, J. R.; Tang, C. W.; Young, R. H. *J. Appl. Phys.* **2003**, *93*, 1108.

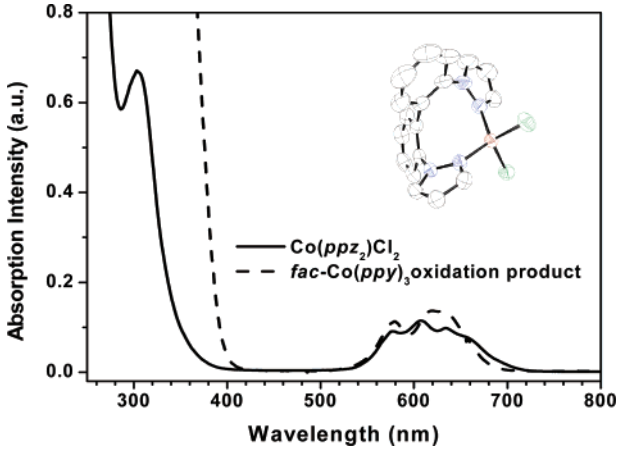

Figure 10. Absorption spectra of the products from the oxidation of *fac*-Co(ppz)$_3$ and *fac*-Co(ppy)$_3$ with (4-BrPh)$_3$NSbCl$_6$. The molecular structure of the Co(ppz$_2$)Cl$_2$ complex is shown in the inset.

atoms coordinate the cobalt center, forming an N_2Cl_2 donor set. The two N−Co−Cl angles (average = 106.98(9)°) are close to those expected for idealized tetrahedral geometry; however, the Cl−Co−Cl and N−Co−N angles are larger (average = 119.71(7)°). A new C−C bond, formed between the two phenyl rings connecting the coordinated pyrazolyl ligands, creates a nine-membered chelate ring. The two Co−N distances (2.025(3), 2.031(3) Å) are slightly longer than those in *fac*-Co(ppz)$_3$, as expected when comparing related bonds on Co(II) and Co(III) centers. The intense blue color of this complex is consistent with a high-spin tetrahedral Co(II) complex. The absorption spectrum taken in acetonitrile displays a characteristic multicomponent band in the 500−700 nm region associated with the $^4T_1 \leftarrow {}^4A_2$ transition in tetrahedral or peudotetrahedral Co(II) complexes (Figure 10).[38] This Co(II) complex is stable in the air for months in its solid state.

The cleavage of cobalt−carbon bonds in organocobalt compounds is not uncommon and has been observed in a variety of Co-catalyzed processes[39] as well as the chemistry of vitamin B_{12}.[40] One of the major pathways of cleavage of cobalt−carbon bonds involves the initial oxidation of the organocobalt(III) compounds, followed by reductive elimination of one or more ligands.[41] It is generally believed that upon increasing the oxidation state of Co, contraction of the Co d-orbitals and reduction in d(Co)−π(C) overlap weaken the Co−C bond and thus promote the subsequent Co−C

Scheme 1

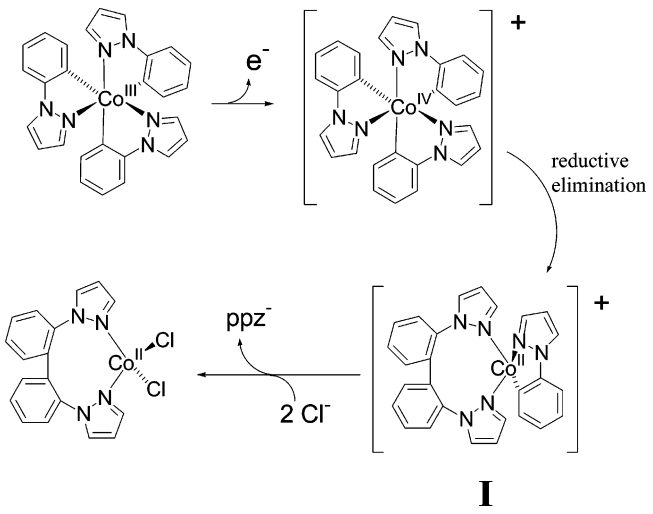

I

cleavage via reductive elimination.[42] A plausible mechanism that would account for the formation of the final product is proposed in Scheme 1. The initial step of the reaction is the chemical oxidation by (4-BrPh)$_3$N$^+$,[43] giving [Co^{IV}(ppz)$_3$]$^+$. Formation of a new bond between the two carbons originally coordinated to the metal suggests that cleavage of the two Co−C bonds is part of a reductive elimination process, forming a mono(organo)cobalt(II) complex with a nine-membered chelate ring. Organocobalt(II) complexes are kinetically labile, typically exchanging organic ligands for anions from solution.[44] Such a ligand exchange would give the neutral product observed here. The chloride ions in the product most likely come from $SbCl_6^-$.[43]

The investigation above implies that decomposition of *fac*-Co(ppz)$_3$ cations might take place during the device operation, leading to the observed rapid degradation in device performance. However, since there are no halide ions in the *fac*-Co(ppz)$_3$ HTL, it is impossible to form the same species that is produced from chemical oxidation. Instead, a likely redox product in a neat thin film could be the penultimate Co(II) complex formed by reductive elimination of two ppz ligands of the Co(IV) complex, labeled **I** in Scheme 1. This tetrahedral intermediate complex would have an N^N-chelating dipyrazolyl ligand (formed by reductive elimination) and a single C^N-chelated ppz ligand. The cationic complex would be expected to efficiently and permanently trap positive charge, leading to severe polarization and increased operating voltages observed as the device degrades.

The higher stability observed for *fac*-Co(ppy)$_3$-based device suggests that *fac*-Co(ppy)$_3^+$ is more stable than the *fac*-Co(ppz)$_3$-based cation. To investigate the difference between cations of *fac*-Co(ppz)$_3$ and *fac*-Co(ppy)$_3$, chemical oxidations of *fac*-Co(ppz)$_3$ and *fac*-Co(ppy)$_3$, using (4-

(38) (a) Cotton, F. A.; Goodgame, M. *J. Am. Chem. Soc*. **1961**, *83*, 1777. (b) Cotton, F. A.; Goodgame, D. M. L.; Goodgame, M.; Sacco, A. *J. Am. Chem. Soc*. **1961**, *83*, 4157.
(39) (a) Rangel, M.; Acros, T.; de Castro, B. *Organometallics* **1999**, *18*, 3451. (b) Dzwiniel, T. L.; Etkin, N.; Stryker, J. M. *J. Am. Chem. Soc*. **1999**, *121*, 10640. (c) Abley, P.; Dockal, E. R.; Halpern, J. *J. Am. Chem. Soc*. **1972**, *94*, 659. (d) Levitin, I.; Sigan, A. L.; Vol'pin, M. E. *J. Chem. Soc., Chem. Commun.* **1975**, 469.
(40) (a) Licht, S. S.; Booker, S.; Stubbe, J. *Biochemistry* **1999**, *38*, 1221. (b) Jarrett, J. T.; Amaratunga, M.; Drennan, C. L.; Scholten, J. D.; Sands, R. H.; Ludwig, M. L.; Matthews, R. G. *Biochemistry* **1996**, *35*, 2462. (c) Hung, R. R.; Grabowski, J. J. *J. Am. Chem. Soc*. **1999**, *121*, 1359.
(41) (a) Abley, P.; Dockal, E. R.; Halpern, J. *J. Am. Chem. Soc*. **1972**, *94*, 659. (b) Levitin, I.; Sigan, A. L.; Vol'pin, M. E. J. C. S. *Chem. Commun*. **1975**, 469.
(42) Chopra, M.; Hun, T. S. M.; Leung, W.-H.; Yu, N.-T. *Inorg. Chem*. **1995**, *34*, 5973.
(43) (a) Bauld, N. L. *Tetrahedron* **1989**, *45*, 5307. (b) Schmittel, M.; Burghart, A. *Angew. Chem., Int. Ed. Engl*. **1997**, *36*, 2550. (c) Nelson, S. F. *Acc. Chem. Res.* **1987**, 269.
(44) (a) Ishikawa, K.; Fukuzumi, S.; Tanaka, T. *Bull. Chem. Soc. Jpn*. **1987**, *60*, 563. (b) Fukazumi, S.; Ishikawa, K.; Tanaka, T. *Organometallics* **1987**, *6*, 358. (c) Costa, G.; Puxeddu, A.; Reisenhofer, E. *J. Chem. Soc., Chem. Commun*. **1971**, 993.

$BrPh)_3N-SbCl_6$, were carried out in parallel and monitored by UV−visible spectroscopy. Evidence of the oxidation reaction was observed in the first scan ($t < 60$ s) for both *fac*-$Co(ppz)_3$ and *fac*-$Co(ppy)_3$. Both complexes displayed a weak, broad band in the near-IR ($\lambda_{max} \sim 950$ nm), consistent with the formation of an intermolecular charge-transfer complex in solution. This band showed a maximum intensity when the $Co(ppz)_3$:$Co(ppz)_3^+$ ratio is 1:1.[45] After 5 min, the $Co(ppz)_3$ sample started showing a broad band centered at 610 nm, and within 40 min the oxidation/rearrangement reaction was complete, giving a spectrum identical to the one shown in Figure 10. The spectral evolution for the $Co(ppy)_3$ sample was very similar to $Co(ppz)_3$; however, the time scale was longer. The first spectrum to show the product peak ($\lambda_{max} = 610$ nm) was taken at $t = 90$ min, and the reaction took more than 4 h to reach completion. The final spectra of the two tetrahedral Co(II) complexes are very similar, consistent with the similar ligand field strength of the dipyrazolylbiphenyl and dipyridylbiphenyl ligands (Figure 10). The increased stability of the $Co(ppy)_3^+$ ion, relative to $Co(ppz)_3^+$, most likely leads to the enhanced stability of $Co(ppy)_3$-based OLEDs.

Conclusion

Novel hole-transporting materials, *fac*-$Co(ppz)_3$, *fac*-$Co(ppy)_3$, and Ga(pma), have been prepared and tested in OLEDs. Using either *fac*-$Co(ppz)_3$ or *fac*-$Co(ppy)_3$ as the bulk hole transporter, and Ga(pma) as the electron-blocking, hole-transporting interfacial layer, highly efficient organic LEDs were realized in which all of the molecular materials used to construct the device are metal complexes. While *fac*-$Co(ppy)_3$ gave stable OLEDs, the *fac*-$Co(ppz)_3$-based devices had very short lifetimes. The most likely cause of the poor device lifetimes is decomposition of the *fac*-$Co(ppz)_3$ cation which leads to severe charge trapping in the operating device.

This study demonstrates the potential of replacing triarylamines with metal complexes as the hole-transporting materials in OLEDs, paving the way for the development of other new hole-transporting materials. This study also points to an important parameter to consider in designing new materials for high efficiency devices. To achieve high efficiency electroluminescence, both carrier and excitons must be confined in the emissive layer of the device. Very weak absorption bands are observed for both Co(III) compounds, assigned to d-d transitions, which can lead to exciton loss from the emissive layer. Such transitions, in the visible part of the spectrum, are common for first-row transition metal complexes, making their use as hole-transporting materials problematic in efficient devices. We are presently examining other metal complexes as hole- and electron-transporting materials, with the goal of eliminating the visible absorption bands. The work presented here leads us to believe that, with the right combination of metal center and ligands, a diverse array of metal complexes can be employed as carrier-transporting materials.

Acknowledgment. The authors thank Dr. K. Dedeian and Rong Yang for helpful discussions. Financial support of this work by Universal Display Corp. and the Defense Advanced Research Projects Agency is gratefully acknowledged.

Supporting Information Available: Results of DFT calculations on *fac*-$Co(ppz)_3$, *fac*-$Co(ppy)_3$, and Ga(pma), crystallographic data in CIF format for *fac*-$Co(ppz)_3$, Ga(pma), and the product of *fac*-$Co(ppz)_3$ oxidation, and the HTL/Ga(pma)/Alq_3 device characteristics (*I* vs *V*, brightness vs *V*, external quantum efficiency vs *V*). This material is available free of charge via the Internet at http://pubs.acs.org.

IC035183F

(45) The point where the ratio of $Co(ppz)_3$ to "$Co(ppz)_3$" was 1:1 was taken as the point where the 350 nm band of the $Co(ppz)_3$ had decreased by a factor of 2. This band bleaches nearly completely in the final product.